JOURNAL OF MATERIALS SCIENCE 27 (1992) 3181–3191

Interfacial properties of fibrous composites

Part II *Determination of interfacial shear strength, interfacial coefficient of friction, and the shrinkage pressure on the fibre*

C.Y. YUE*
School of Mechanical and Production Engineering, Nanyang Technological University, Nanyang Avenue, Singapore 2263

W. L. CHEUNG
Department of Mechanical Engineering, University of Hong Kong, Pokfulam Road, Hong Kong

It is shown that the interfacial parameters of a composite system which include the interfacial shear strength, the interfacial coefficient of friction, and the shrinkage pressure can be determined using the proposed model for the debonding and pull-out processes. The effect of the matrix morphology and the fibre surface treatment on the interfacial parameters, and hence on the mechanical properties, for a glass fibre–polypropylene system was determined.

1. Introduction

The present work is the second in a series on the interfacial properties of fibre-reinforced composites. The models for debonding crack initiation and for the fibre pull-out process developed in an earlier paper [1] are utilized to determine the interfacial parameters of a composite system. The interfacial parameters such as the interfacial shear strength, τ_i, the interfacial frictional stress, τ_f, the interfacial coefficient of friction, μ, and the shrinkage stress of the matrix on the fibre, P_0, are important because they affect the strength and toughness of the composite.

The theoretical basis for such determination will first be outlined. The applicability of the above technique to a glass fibre–polypropylene system will then be considered. Finally, the effect of the interfacial matrix morphology and the silane treatment of the fibre on the interfacial parameters will be determined.

The distinguishing feature of the proposed model [1] is that in contrast to existing techniques, all three parameters, τ_i, μ, and P_0, can be determined from only one set of pull-out data. To achieve this, pull-out specimens with slightly tapered fibres must be utilized. At present, the interfacial shear strength, τ_i, can readily be determined from existing techniques which employ pull-out specimens with fibres of constant diameter. However, separate tests based on either the photoelastic method [2] or the single fibre pull-out test with externally applied pressure on the pull-out specimens [3, 4] must be utilized to evaluate P_0 and μ. The former method which is only applicable to photoelastic matrix systems cannot determine μ and cannot be used for many composite systems. In addition, the application of pressure to the pull-out specimen during testing in the latter method is difficult to achieve. The new proposed model does not suffer from these inadequacies.

2. Theory

2.1. Determination of interfacial shear strength, τ_i

The interfacial shear strength, τ_i, can be determined from the plot of the maximum debonding force, F_d, against the embedded fibre length, L. A typical plot of F_d against L is as shown in Fig. 1, where L_c is related to the critical transfer length. Two methods can be developed.

2.1.1. Method I

This is based on the determination of the slope of the plot of F_d against L at $L = 0$. The theoretical basis of this method is as follows. In Fig. 1, within the region $L < L_c$, complete debonding would occur catastrophically [1] once the crack has initiated. Hence, for specimens with $L < L_c$, F_d is governed only by the maximum shear stress criterion [1] and is equal to the force for crack initiation, F_i, where

$$F_d = F_i = 2\pi r\tau_i\left[\alpha(1-\psi)\exp(-\alpha L) + [\psi + (1-\psi)\exp(-\alpha L)]\frac{\alpha\cosh\alpha L}{\sinh\alpha L}\right]^{-1} \quad (1)$$

where $\alpha = K_a^{1/2}$, r is the radius of the fibre, and K_a and ψ are constants [1] which are dependent on the specimen geometry and the moduli of the matrix and fibre. The initial slope of the plot can be determined by

* Author to whom all correspondence should be addressed.

0022–2461

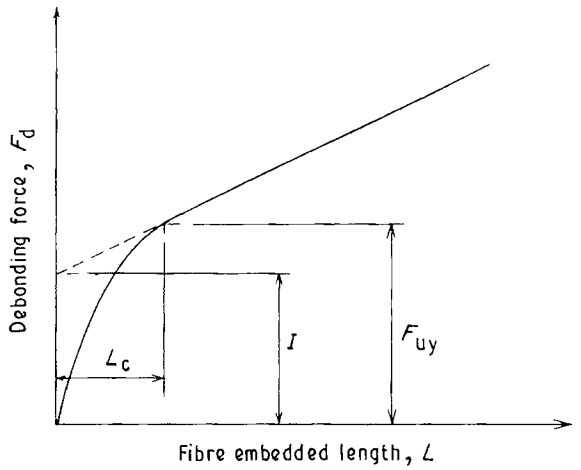

Figure 1 Plot of the debonding force, F_d, against the embedded length, L.

differentiating Equation 1 to give

$$\left(\frac{dF_d}{dL}\right)_{L=0} = \left\{\frac{2\pi r\tau_i[(1-\psi)\cosh\alpha L + \psi]}{[(1-\psi)+\cosh\alpha L]^2}\right\}_{L=0} \quad (2a)$$

or

$$\left(\frac{dF_d}{dL}\right)_{L=0} = 2\pi r\tau_i \quad (2b)$$

Therefore

$$\tau_i = \frac{1}{2\pi r}\left(\frac{dF_d}{dL}\right)_{L=0} \quad (3)$$

It is apparent that τ_i can be determined from the slope of the plot at $L = 0$.

2.1.2. Method II

This method is appropriate to composite systems with very short L_c, such that the initial slope at $L = 0$ is difficult to measure experimentally due to the lack of data points and a very small region of $0 < L < L_c$. This situation would arise [1] in composite systems with low interfacial strength. It can be seen from Fig. 1 that

$$F_{uy} = I + L_c\left(\frac{dF_d}{dL}\right)_{L\geq L_c} \quad (4a)$$

where I is the intercept on the vertical F_d axis. Substituting for $F_{uy} = 2\pi r\tau_i/N$ and taking the length of the remaining bonded (i.e. undebonded) region to be L_c [1], the above equation becomes

$$2\pi r\tau_i N^{-1} = I + L_c\left(\frac{dF_d}{dL}\right)_{L\geq L_c} \quad (4b)$$

where

$$N = \alpha(1-\psi)\exp(-\alpha L_c) + \alpha[\psi + (1-\psi)\exp(-\alpha L_c)]\coth\alpha L_c \quad (4c)$$

Because L_c is a constant which is dependent on τ_i, the only unknown factor in Equation 1 is τ_i. The exact solution to the equation is not a simple expression. However, τ_i can be determined using the iterative method provided the intercept, I, and the slope at $L = L_c$ are known.

If τ_i is considerably larger than the interfacial frictional stress τ_f, the intercept, I, will be large and the above methods will allow accurate determination of τ_i. (The interfacial frictional stress is the stress acting between the debonded surfaces of the pull-out specimen or the debonded fibre–matrix interfaces during the pull-out process.) However, the intercept, I, will diminish as τ_i decreases. For the case where τ_i is small, such that $\tau_i = \tau_f$, the intercept vanishes completely and the plot of F_d against L (see Fig. 1) becomes a straight line through the origin. Therefore, τ_i cannot be evaluated directly but can be obtained by determining τ_f. It should be pointed out that τ_i is usually larger than τ_f in most practical composite systems so that the above methods are applicable.

2.2. Determination of the interfacial frictional stress, τ_f

It has been shown [1] for any system with $L > L_c$ that the pull-out force, F_p, is given by

$$F_p = 2\pi r\tau_i\left[\alpha(1-\psi)\exp(-\alpha l_u) + [\psi + (1-\psi)\exp(-\alpha l_u)]\frac{\alpha\cosh\alpha l_u}{\sinh\alpha l_u}\right]^{-1} + 2\pi r P_0\mu(L - l_u) \quad (5)$$

where l_u is the length of the interface which had not debonded. The slope of the plot of F_d against L at any point x can be determined by differentiating Equation 5. For a rigid fibre system in the region $L > L_c$, the differential of the first term on the right of Equation 5 can be neglected, and the slope of the plot of F_d against L is

$$\left(\frac{dF_d}{dL}\right)_{L>L_c} = 2\pi r P_0\mu \quad (6)$$

Therefore

$$\tau_f = P_0\mu = \frac{1}{2\pi r}\left(\frac{dF_d}{dL}\right)_{L>L_c} \quad (7)$$

Hence, the interfacial frictional stress, τ_f, can be determined from the slope of the plot at $L > L_c$. However, this method tends to underestimate τ_f because, in practice, the fibre does suffer from some Poisson shrinkage under the applied load. If Poisson shrinkage or contraction is significant, the region of the curve beyond L_c would become curved [1] and the above method would not be applicable.

2.3. Determination of μ and P_0

Let the work done in extracting a tapered fibre from a pull-out specimen be denoted by W and the work done in extracting a constant diameter fibre be W_0. It has been shown in an earlier work [1] that the extra work expended in extracting a tapered fibre (compared to the work required to extract a embedded

TABLE I Types of glass fibre–polypropylene pull-out specimens considered

Specimen	Fibre surface treatment			Cooling condition
	Treatment solution	Dipping time	Drying condition	
CF-WQ	–	–	–	Water quenched
CF-AC	–	–	–	Air cooled
CF-50C	–	–	–	50 °C oven cooled
TF-WQ	1% silane	5 s	Room	Water quenched
TF-AC	1% silane	5 s	Room	Air cooled
TF-50C	1% silane	5 s	Room	50 °C oven cooled
TF(4B)-WQ	1% silane	4 min	Blow dry	Water quenched
TF(40)-WQ	1% silane	4 min	100 °C oven treated	Water quenched

fibre of constant diameter) is represented by the shaded region of the pull-out curve in Fig. 2. This extra work done ($W - W_0$) is given by

$$W - W_0 = \frac{\pi r E_{mc} \tan\theta}{R(1 + \nu_m)} \left\{ \frac{L^2}{2} - \frac{rL}{2\mu R} + \left(\frac{r}{2\mu R}\right)^2 \times \left[1 - \exp\left(\frac{-2\mu RL}{r}\right)\right] \right\} \quad (8a)$$

where E_{mc} is the compressive modulus of the matrix, θ is the angle of taper and is positive, $R = (E_{mc}\nu_f)/E_f(1 + \nu_m)$, ν_f and ν_m are the Poisson's ratios of the fibre and matrix, respectively, and E_f is the modulus of the fibre. For a rigid fibre system such as the glass fibre–polypropylene system in which the modulus of the fibre is much larger than that of the matrix, Equation 8a reduces to

$$W - W_0 = \frac{\pi\mu E_{mc} \tan\theta}{3(1 + \nu_m)} L^3 \quad (8b)$$

Apart from the interfacial coefficient of friction, μ, other parameters in Equation 8b can be obtained experimentally. Therefore, μ can be calculated from a knowledge of $W - W_c$, where

$$\mu = \frac{3(1 + \nu_m)(W - W_0)}{\pi E_{mc} L^3 \tan\theta} \quad (9)$$

But [5] $W_0 = \pi r \mu P_0 L^2$. Thus, the parameter P_0 can then be determined by substituting the value of μ into the expression for W_0 where

$$P_0 = \frac{W_0}{\pi r \mu L^2} \quad (10)$$

W_0 can readily be obtained from the experimental pull-out force/displacement plot.

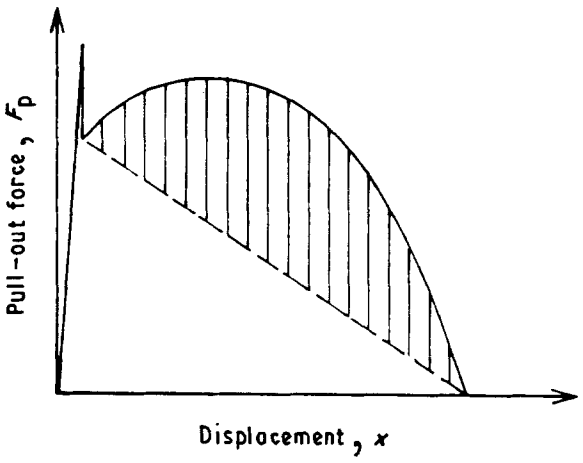

Figure 2 Extra frictional work done (shaded area) due to pull-out of a slightly tapered fibre with $\tan\theta > 0$.

3. Experimental procedure

3.1. Materials and specimens

The polypropylene (PP) used was Shell Chemicals KM6100 while the silane coupling agent used was Dow Corning's Z-6032. The tapered fibres as well as constant diameter glass fibres were prepared from E-glass rods in the laboratory. The average fibre diameter was 200 μm. All specimens were compression moulded at 250 °C for 8 min and then cooled according to the required conditions. Eight specimen types were tested in the present work:

(a) clean (untreated) fibre in a water quenched PP matrix (CF-WQ);

(b) clean fibre in an air-cooled matrix (CF-AC);

(c) clean fibre in the 50 °C oven-cooled matrix (CF-50C);

(d) silane-treated fibre in a water-quenched matrix (TF-WQ);

(e) silane-treated fibre in an air-cooled matrix (TF-AC);

(f) silane-treated fibre in the 50 °C oven-cooled matrix (TF-50C);

(g) silane-treated blower-dried fibre in water- quenched matrix TF(4B)-WQ;

(h) silane-treated oven-dried fibre in water-quenched matrix TF(4O)-WQ.

Additional information of the silane treatment of the treated fibres is given in Table I. Specimens of different embedded fibre lengths were prepared. The pull-out tests were conducted on an Instron testing machine at a crosshead speed of 5 mm min^{-1} and a chart speed of 100 mm min^{-1}. The matrix blocks in the air-cooled and 50 °C oven-cooled specimens were cloudy, while that in the water-quenched specimens were clear and fairly transparent. The onset and propagation of the debonding crack at the interface of the latter specimens could be seen visually [5] during the tests. Details of the preparation of the fully supported single fibre pull-out specimens and the testing procedure are outlined elsewhere [6].

3.2. Specimen characterization

The degree of taper of each extracted fibre was measured after the pull-out test on an X–Y table utilizing the graduated objective lens of the optical microscope on a Shimadzu microhardness tester. The graduations on the lens were spaced 0.5 μm apart. The glass fibre was sputter coated with gold–palladium before it was placed on a mirror and viewed under the microscope. The coated fibre provided strong contrast so that the fibre diameter could readily be measured. The fibre diameters, D_1 and D_2, at the fibre-embedded end and the fibre-emergent end, respectively, as well as the distance between the above two readings, S, were measured. The degree of taper, $\tan\theta$, could be calculated from the relationship, $\tan\theta = D_1 - D_2/S$. Typical values of $\tan\theta$ varied between -4×10^{-4} and 4×10^{-4}.

The size of the spherulites in the water-quenched, air-cooled, and 50 °C oven-cooled PP matrices were determined from polarized light micrographs of microtomed films of the matrices. Thermal analysis of the respective matrices was conducted using the DuPont 9900 differential scanning calorimeter (DSC) at a scan rate of 5 °C min^{-1} to 180 °C. The degree of crystallinity was calculated by assuming the heat of fusion [7] of 100% crystalline PP to be 138.2 J g^{-1}.

3.3. Compressive modulus

The dependence of the compressive moduli of the water-quenched, air-cooled, and 50 °C oven-cooled PP matrices on strain rate was determined in order to facilitate the calculation of P_0 and μ for the respective specimen types. The compression test specimens were machined from the matrices of the pull-out specimens which had been tested. Each compression test specimen was 12.7 mm high, 12.7 mm wide, and 3.4 mm thick. The specimens were compressed along their height. Crosshead speeds of 0.1, 0.5, 1.0, 3.0, and 5.0 mm min^{-1} were used and the strain rate was taken to be the crosshead speed divided by the original height of the specimen.

3.4. Measurement of work done

The total work done, W, due to frictional pull-out and the extra work, $W - W_0$, expended arising from the use of a slightly tapered fibre with a positive $\tan\theta$ were measured as follows. The area which corresponded to the work done was cut and weighed using an electronic balance which was accurate to 0.1 mg. The work done was then calculated by comparing the weight of the above area with the weight of a square section of known area cut from the same paper.

4. Results and discussion

4.1. Matrix morphology and compressive modulus

The average spherulite size and the degree of crystallinity of the different matrices are as shown in Table II. It is apparent that the spherulite size of the water-quenched matrix is considerably smaller than those of the air-cooled and 50 °C oven-cooled PP. As expected, the WQ matrix which had the highest cooling rate had the lowest crystallinity.

TABLE II Spherulite size and degree of crystallinity of polypropylene matrix

	Cooling condition		
	WQ	AC	50 °C
Spherulite diameter (μm)	64	280	372
Crystallinity	60.8	66	68.7

The change in compressive modulus, E_{mc}, of the PP matrices with compressive strain rate is as shown in Fig. 3. As expected, the WQ PP matrix which had the lowest crystallinity had the lowest modulus. The air-cooled matrix and the 50 °C oven-cooled matrix had moduli which were similar as they had a similar degree of crystallinity. The actual compressive moduli of the latter specimens may be slightly higher than that in Fig. 6 because small inter-spherulitic voids which were present in these matrices may have resulted in a lower value of the measured moduli. Such inter-spherulitic voids caused the latter matrices to appear milky. In contrast, the WQ matrix was clear and transparent because no such voids were present.

It can be seen from Fig. 3 that E_{mc} is very strain-rate dependent and almost doubled within the range of strain rates used. It is therefore imperative to use the correct value of E_{mc} to calculate P_0 and μ. When the slightly tapered fibre is being extracted at a given crosshead speed, the matrix around the fibre is compressed at a strain rate which is dependent on the degree of taper of the fibre. The compressive strain rate, $\dot{\varepsilon}$, on the matrix around the fibre was taken to be $\dot{\varepsilon} = D \tan\theta / r$, where D is the crosshead speed which was 5 mm min^{-1}. The value of E_{mc} for each specimen was determined from Fig. 3 using the above relationship for compressive strain rate.

4.2. Characteristics of the pull-out curves

Some typical experimental pull-out curves for both the treated and untreated fibre specimens are as

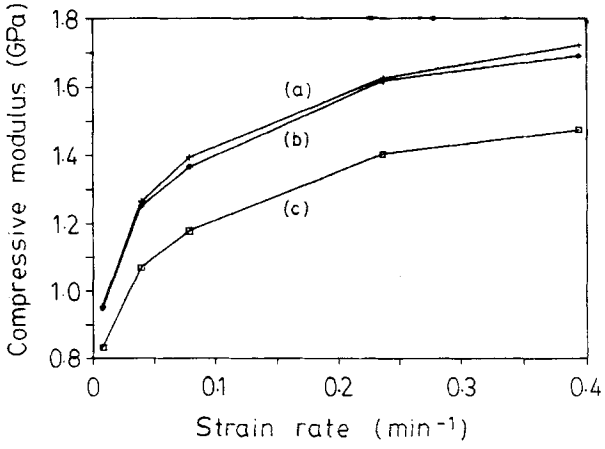

Figure 3 Variation of compressive modulus of polypropylene matrix with strain rate: (a) AC air cooled, (b) 50 °C oven cooled, (c) WQ water quenched.

shown in Fig. 4 In general, there are three distinct regions in the pull-out curves. The first region, Region I, is that from the starting point up to the point where F_p reaches a maximum. The position where the pull-out force, F_p, is a maximum corresponds to the point at which complete debonding of the fibre–matrix interface occurred. This is followed immediately by a short region (Region II) where F_p decreases rapidly and unsteadily. The final region (Region III) where F_p decreases steadily, corresponds to the stage where the debonded fibre is being progressively extracted from the matrix block. The stick–slip phenomenon was sometimes manifest in the second region (see Fig. 4b) in the treated fibre specimens. This is in contrast to fibre-reinforced thermoset systems where the stick–slip phenomenon is manifest in both Regions II and III.

4.2.1. Treated fibre specimens

Initially, the fibre–matrix interface was intact and it can be seen from Fig. 4a that F_p increased linearly with the displacement. When F_p reached F_i, interfacial debonding initiated at the fibre emergent end due to high stress concentration in this region [1]. The initiation of the interfacial debonding caused a drop in the pull-out force immediately after F_i. Thereafter, F_p continued to increase with the pull-out displacement as the debonding crack continued to propagate towards the fibre embedded end.

The point of debonding crack initiation appears as a step or discontinuity in Region I (see Fig. 4a). Such crack initiation could be observed visually in the water-quenched specimens. The above step exists in the pull-out curves of almost all the treated fibre specimens and is more apparent when chart speeds of 100 mm min^{-1} or more are used.

Occasionally, in about 10% of the treated fibre specimens, striations due to the stick–slip phenomenon existed in the pull-out curves. This phenomenon occurred more frequently in specimens with long fibre embedded lengths and long fibre-free lengths. The former specimen condition would lead to a higher frictional force during fibre pull-out, while the latter condition increases the stored energy in the system. It appears that momentary relaxation of the higher frictional force or larger stored energy in the system in these specimens during the "slip" stage of the phenomenon gives rise to the pronounced striations in the curves.

4.2.2. Two debonding cracks

In treated fibre specimens with long embedded length, L, a second debonding crack sometimes initiated at the fibre-embedded end whilst the first debonding crack which had initiated at the fibre-emergent end continued to grow (in Region I). The distinct initiation of the second debonding crack was observed visually in TF-WQ specimens with $L > 8$ mm. The two debonding cracks propagated in opposite directions and met somewhere along the fibre-embedded length as the pull-out force was increased.

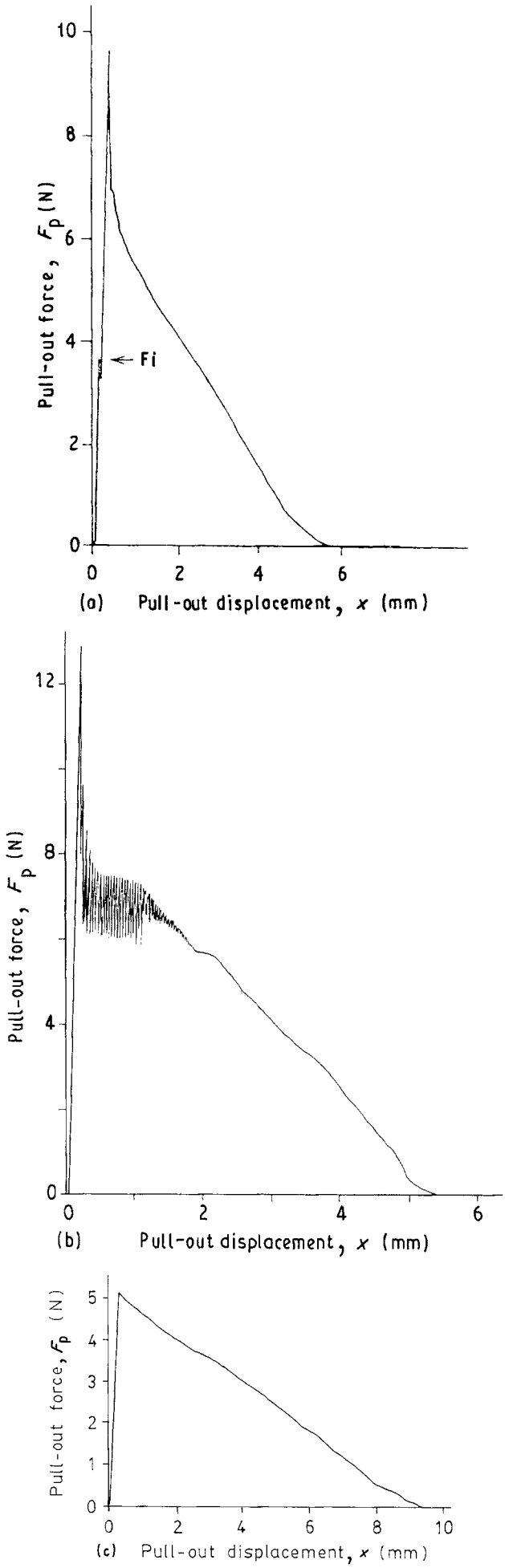

Figure 4 Typical experimental pull-out curves: (a) TF-WQ, $d = 185$ μm, $L = 5.6$ mm; (b) TF-WQ, $d = 233$ μm, $L = 5.5$ mm; (c) CF-WQ, $d = 196$ μm, $L = 9.2$ mm (d is the fibre diameter).

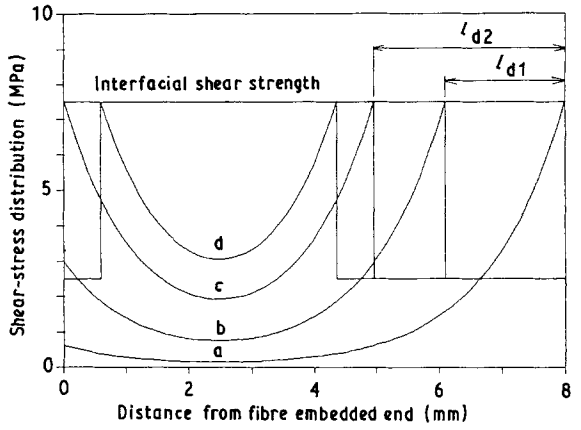

Figure 5 Schematic representation of variation of theoretical shear stress distribution along an embedded fibre at different stages of the pull-out test, $L = 8$ mm. F_p: (a) 6.2 N; (b) 10.9 N; (c) 15.9 N; (d) 17.1 N.

The above phenomenon can be accounted for using the model developed earlier [1]. It can be shown [5] that the shear stress concentration at the fibre-embedded end of the fibre increases when the bonded area is being continuously depleted as the first debonding crack advances. The schematic representation of the change in shear-stress distribution along the fibre as the first debonding crack advances from the fibre-emergent end is as shown in Fig. 5. The expression for the shear stress [1] along the part of the interface which is still intact is given by

$$\tau_x = \frac{F_p}{2\pi r}\left\{\alpha(1-\psi)\exp(-\alpha x) + [\psi + (1-\psi)\exp(-\alpha L)]\frac{\alpha\cosh\alpha x}{\sinh\alpha L}\right\} \quad (11)$$

To obtain the shear stress distributions in Fig. 5, the physical and geometrical parameters of the glass fibre–polypropylene system in the present work was substituted into Equation 11. The actual values of the parameters used is given elsewhere [1]. The single fibre pull-out specimen was assumed to be loaded to different load levels at different stages of the advancement of the crack, and the shear stress distributions at the different stages are as shown in Fig. 5.

If the interfacial shear strength, τ_i, is assumed to be 7.5 MPa, then the regions in Fig. 5 where τ_x is greater than 7.5 MPa corresponds to regions which had debonded. For example, Curve b shows the shear-stress distribution after the crack had advanced through a distance, l_{d1}. The shear stress at the tip of the advancing crack was assumed to be maintained at τ_i. As the crack propagates, the stress distributions change as shown from Curves a–d. It is apparent from Curve C that the shear stress at the fibre emergent end (i.e. at $x = 0$ mm) has increased to τ_i when the crack had propagated a distance l_{d2}. A further increase in the applied force, F_p, would result in the formation of a second debonding crack at the fibre embedded end (see Curve d) as observed experimentally.

4.2.3. Untreated fibre specimens

A typical pull-out curve of the untreated (clean) fibre specimens is as shown in Fig. 4c. In contrast to the curves of the treated fibre specimens (cf. Fig. 4a), there is no step or discontinuity in Region I of the pull-out curve even when a chart speed of 100 mm min^{-1} was used. This suggests that there is no distinct point for the initiation of the debonding crack in the untreated specimens. Furthermore, no Region II exists because there is no rapid drop in the pull-out force when the maximum value of F_d was reached. Hence, extraction of the fibre from the matrix commences immediately after this point.

The above observations suggests that the interfacial shear strength in the clean fibre specimens is very low. This can probably be attributed to the limited contact between PP and the glass fibre at the interface [6] and to the poor adhesion of PP of glass. The actual contact between the PP and glass at the interface is rather limited due to some debonding caused by directional shrinkage of the spherulites which gives rise to the presence of kink bands [8].

4.2.4. Shape of the pull-out curves

A wide range of experimental pull-out curves from specimens with different degree of taper (i.e. different $\tan\theta$) are as shown in Fig. 6. The shape of the experimental curves vary with the value of $\tan\theta$ in the manner predicted by the theoretical model [1]. This implies that the theory [1] can be utilized to determine the values of the interfacial parameters τ_i, P_0, and μ.

There are a number of minor aspects of the experimental curves which were not accounted for in the development of the theory. Firstly, the undulating nature of the interface in some clean fibre (CF-AC, and CF-50C) specimens [8] may cause the matrix shrinkage pressure, P_0, to vary along the embedded fibre length. Under these conditions, the pull-out curve of these specimens would not be smooth (see Fig. 6c). Secondly, although the tensile stress on the fibre is greatest along its free length, fibre breakage may sometimes occur inside the matrix due to surface flaws on the embedded length (see Fig. 6g). The sudden drop of F_p in Fig. 6g corresponds to the instant at which fibre breakage occurred inside the matrix. The remainder of the curve in Fig. 6g corresponds to the extraction of the broken fibre from the matrix.

In general, the fibres utilized in the specimens should not have large positive values of $\tan\theta$, otherwise fibre breakage is likely to occur and complete extraction of the fibres would not be possible. In fact, pull-out curves for specimens with large positive $\tan\theta$ should not be utilized for the analysis. This is because contact between the debonded fibre and the matrix would not approach the pure sliding friction condition assumed in the theory. A large ploughing friction component due to significant deformation of the matrix layer by the fibre would also exist in these specimens and thus give rise to inaccurate analysis.

4.3. Interfacial coefficient of friction, μ, and matrix shrinkage pressure, P_0

Only experimental curves of specimens with $\tan\theta$ of between 2×10^{-4} and 4×10^{-4} and long embedded

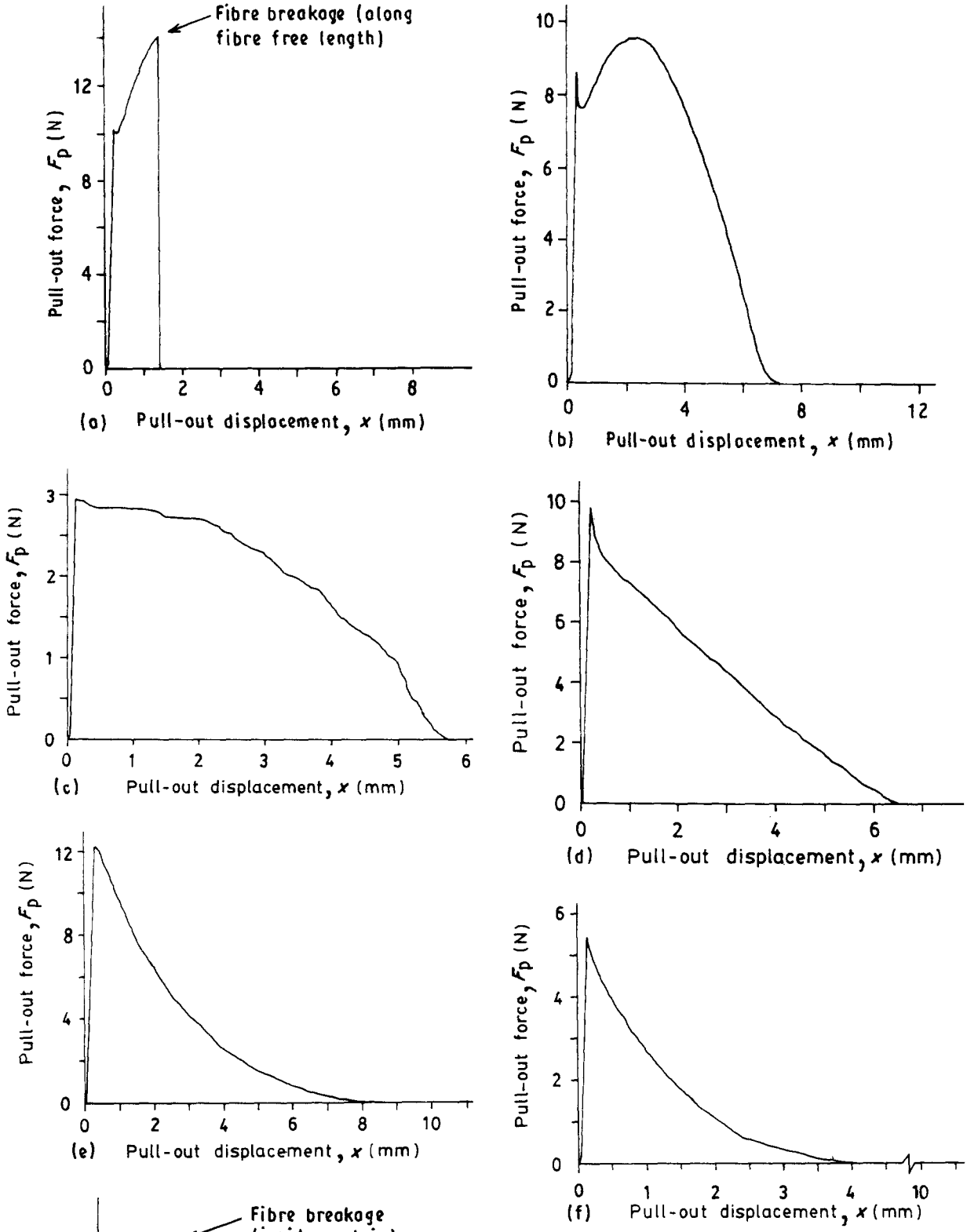

Figure 6 Typical experimental pull-out curves: (a) TF-AC, $d = 203\ \mu m$, $\tan\theta > 0$, $L = 8.0$ mm; (b) TF-WQ, $d = 185\ \mu m$, $\tan\theta = 4.4 \times 10^{-4}$, $L = 6.6$ mm; (c) CF-AC, $d = 204\ \mu m$, $\tan\theta = 2.3 \times 10^{-4}$, $L = 5.6$ mm; (d) TF-50C, $d = 190\ \mu m$, $\tan\theta = 0.3 \times 10^{-4}$, $L = 6.7$ mm; (e) TF-50C, $d = 190\ \mu m$, $\tan\theta = -1.8 \times 10^{-4}$, $L = 8.4$ mm; (f) CF-AC, $d = 210\ \mu m$, $\tan\theta = -4.0 \times 10^{-4}$, $L = 9.5$ mm, (g) CF-AC, $d = 235\ \mu m$, $\tan\theta > 0$, $L = 9.5$ mm.

lengths ($L > 4$ mm) were used to calculate P_0 and μ. This is because the extra work done due to $\tan\theta$ could be determined accurately in these specimens because the onset of frictional pull-out was more distinct in these curves. Typical values of μ and P_0 for some

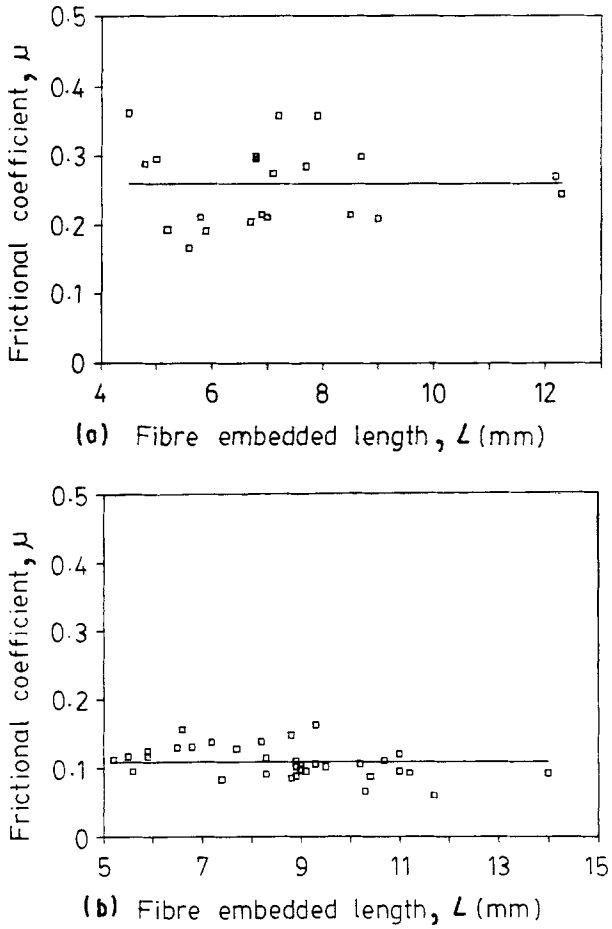

Figure 7 Values of interfacial coefficient of friction, μ, for specimens with different embedded lengths L: (a) TF-WQ, (b) CF-AC.

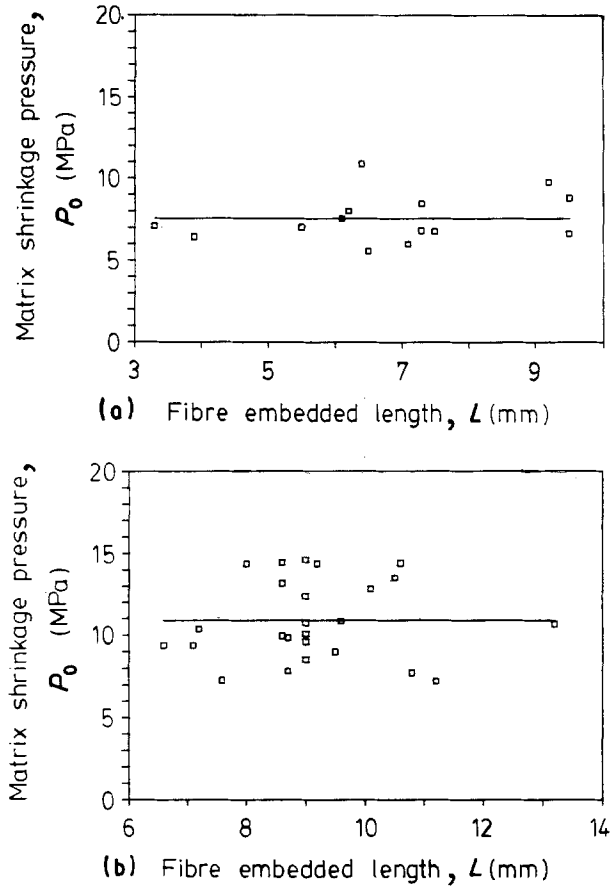

Figure 8 Values of matrix shrinkage pressure, P_0, for specimens with different embedded lengths L: (a) TF-AC, (b) CF-WQ.

specimens calculated using Equations 9 and 10, respectively, are as shown in Figs 7 and 8. The horizontal lines in the above figures indicate the average values of the data in each plot.

There is some scatter in the data for μ and P_0. This is to be expected because the amount of extra work done is dependent on the nature and plane of interfacial failure which can vary [6] from specimen to specimen. Difficulties in determining the precise value of tan θ of the slightly tapered fibres also contribute to some of the scatter. However, reliable average values of μ and P_0 could be determined by acquiring more test data as shown in Figs 7 and 8. The average values of μ and P_0 for the different specimens are as shown in Table III.

4.3.1. Factors which affect μ and P_0

It can be seen from Table III that the matrix shrinkage pressure, P_0, in the water quenched specimens (CF-WQ, TF-WQ) is higher than that in the air-cooled and 50 °C oven-cooled specimens. This is to be expected because the rapid cooling in the CF-WQ and TF-WQ specimens would suppress crystallization and lead to a matrix with a high degree of entanglement and high internal residual stress. There is little difference in P_0 between the air-cooled (CF-AC, TF-AC) and oven-cooled (CF-50C, TF-50C) samples due to the small difference in cooling rates between these specimens.

It is further apparent from Table III that P_0 is only dependent on the cooling rate and not the fibre surface treatment. This is because the silane coat on the surface of the treated fibres cannot relieve the residual shrinkage stress at the fibre–matrix interface.

The interfacial coefficient of friction, μ, is constant for a given fibre surface treatment (see Table III). This is to be expected as μ is dependent on the nature and properties of the sliding surfaces (debonded surfaces) which are in contact with each other when the fibre is

TABLE III Interfacial parameters of the specimens; interfacial coefficient of friction, μ, shrinkage pressure on the fibre, P_0, and the interfacial frictional stress, τ_f

	CF-WQ	CF-AC	CF-50C	TF-WQ	TF-AC	TF-50C
μ	0.09	0.11	0.09	0.26	0.33	0.34
P_0(MPa)	10.9	7.85	8.30	11.2	7.55	7.72
τ_f(MPa)	0.92	0.81	0.74	2.55	2.13	2.20
μP_0(MPa)	0.98	0.86	0.75	2.91	2.49	2.62

TABLE IV Interfacial shear strength, τ_i, and the critical fibre length, L_c

Specimen	CF-WQ	CF-AC	CF-50C	TF-WQ	TF-AC	TF-50C
τ_i(MPa)	0.92[a]	0.81[a]	0.74[a]	7.5	5.0	4.5
L_c(mm)	–	–	–	1.3	1.0	1.0

[a] Assuming $\tau_i = \tau_f$.

being extracted from the matrix. The type of debonded surfaces at the interface is dependent on the plane of failure, which in turn is dependent [6] on the fibre surface treatment.

It has been shown [6] that interfacial failure in the untreated clean fibre (CF) specimens occurred at the fibre–PP interface, whilst that in the treated fibre (TF) specimens mainly occurred at the silane–PP interface. There were very little matrix residues on the surfaces of the extracted fibres in the CF specimens. In contrast [6], interfacial failure in the TF specimens sometimes occurred within the bulk PP matrix such that matrix residues remained on the extracted fibre surface. Therefore, the CF specimens would have a smaller μ compared to the TF specimens. This is in agreement with the experimental results in Table III which indicate that the fibre surface treatment caused a three-fold increase in μ.

Moreover, the TF-AC and TF-50C specimens usually had larger residues than the TF-WQ specimens [5]. Hence, for the TF samples, it would be relatively easier to extract the fibre in the WQ specimen, and μ for the TF-WQ specimens is expected to be smaller than that for the TF-AC and TF-50C specimens. This is also in agreement with the results in Table III. (It is important to note that μ is not a "true" coefficient of friction but is simply a parameter which is utilized to describe the macroscopic or average frictional properties of the debonded surfaces which are in contact with each other during the fibre extraction process. This is because the nature and character of the debonded surfaces in the TF specimens are not uniform or homogeneous.)

4.4. Plots of debonding force, F_d against the embedded length, L

The plots of F_d against L for the TF specimens are as shown in Fig. 9a–c. It can be seen that F_d initially increases rapidly with the fibre embedded length until it reaches a distinct knee at about $L = 1$ mm. Thereafter, a linear relationship exists between F_d and L. In the region on the left of the knee, $L < L_c$ and the maximum debonding force F_d is governed [1] by the maximum interfacial shear stress criterion. As predicted [1], specimens with $L < L_c$ failed catastrophically immediately after the debonding crack had initiated.

The region on the right of the knee in Fig. 9a–c corresponds to the case where $L > L_c$. In this region, the debonding crack has [9] a distinct initiation and propagation stage and F_d is mainly dependent on the friction between the fibre and the matrix. It can be seen (Fig. 9a–c) that F_d increases almost linearly with L. This is to be expected [1] for the glass fibre–PP system considered where the modulus of the fibre is considerably higher than that of the matrix. The interfacial frictional stress, τ_f, can therefore be calculated from the slope of the plot in the region where $L > L_c$.

The plots of F_d against L for the untreated CF specimens are as shown in Fig. 9d–f. Unlike the TF specimens, no knees exist in the plots, and the curves consist of straight lines through the origin. The magnitude of τ_f for the CF specimens can similarly be determined from the slope of the plots. However, the absence of knees in these plots indicate [1] that the interfacial shear strength, τ_i, is low and is only marginally higher than τ_f.

4.5. Interfacial frictional stress, τ_f

The magnitude of τ_f for the specimens as determined from the slopes in Fig. 9a–f using a linear regression method are as listed in Table III. The regression lines are shown in Fig. 9. In a rigid fibre system such as the glass fibre–PP presently considered, τ_f is also equal [1] to P_0 multiplied by μ. The values of P_0, μ, and the multiple (μP_0) are also given in Table III. It is apparent from Table III that there is good agreement between the values of τ_f determined from the two independent methods. This indicates that the results in Table IV and hence the theoretical model for interfacial debonding [1] are reliable.

It can be seen (Table III) that the values of τ_f for the treated fibre specimens obtained from the slopes of Fig. 9a–c were consistently slightly lower than those determined from P_0 and μ. This difference can be accounted for in terms of the different extent of Poisson shrinkage in the fibres. The stress levels associated with the debonding initiation and propagation stages (from which data of the slope of F_d against L are obtained) are higher than the stress levels associated with the pull-out stage (from which data for calculating P_0 and μ are obtained). Consequently, the extent of Poisson shrinkage in the former would be larger than that in the latter. Therefore, the value of τ_f determined from the former method would be affected more adversely (τ_f would be lower) than that determined from the latter method. This is in agreement with the results in Table III.

4.6. Interfacial shear strength, τ_i, and critical fibre length, L_c

As L_c is very short (less than 1 mm, see Fig. 9), Method II was utilized to calculate τ_i and L_c. The values of τ_i and L_c are as shown in Table IV. The interfacial strength, τ_i, of the untreated CF specimens could not be determined because L_c for these plots are too small. Nevertheless, τ_i for the CF specimens may be taken to

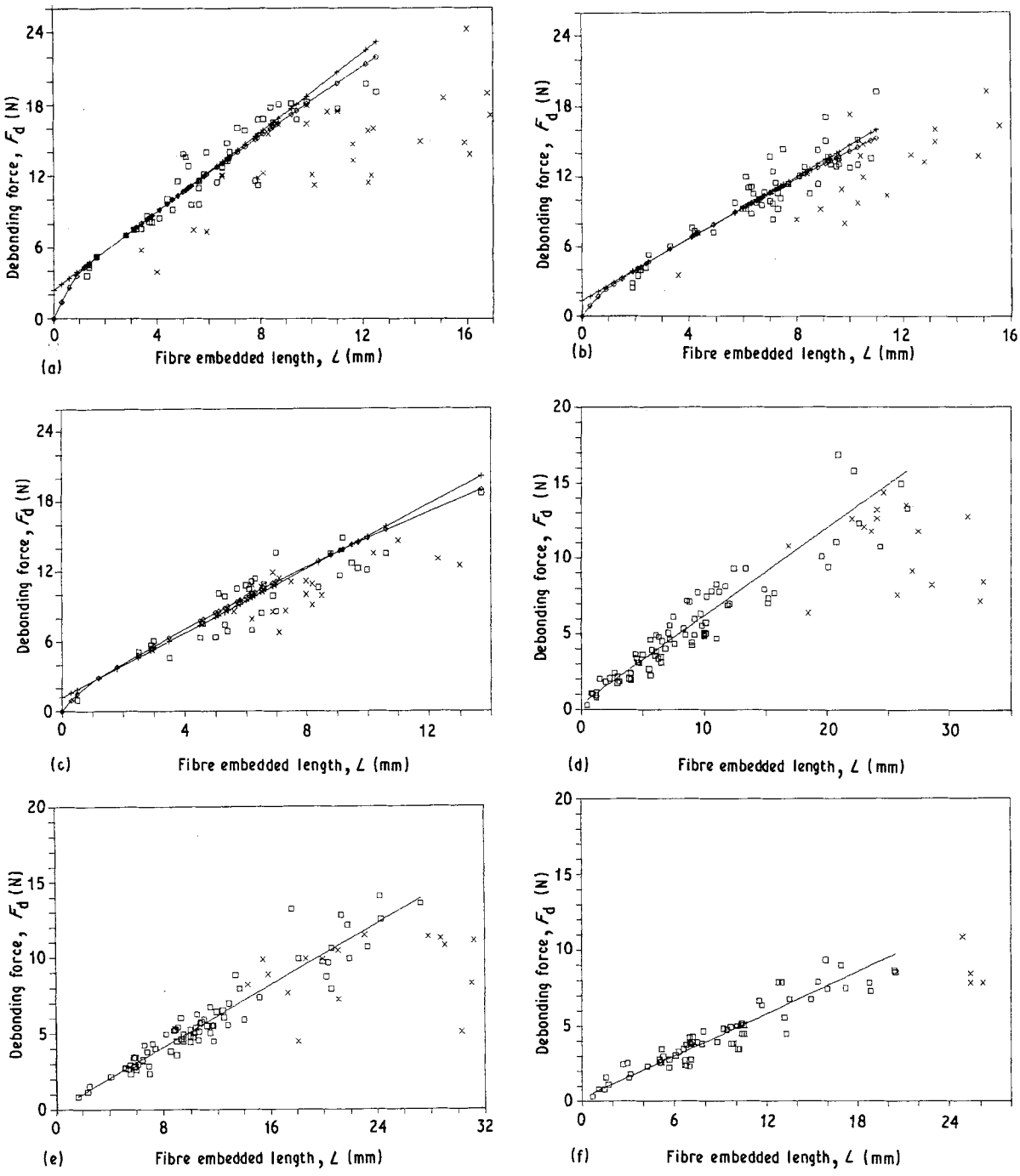

Figure 9 Plots of debonding force F_d against fibre embedded length, L: (□) fibre pull-out, (×) fibre breakage, (+) linear regression line, (◇) theoretical curve. (a) TF-WQ, (b) TF-AC, (c) TF-50C, (d) CF-WQ, (e) CF-AC, (f) CF-50C.

be equal to τ_i. This is because the shallow drop in pull-out force after complete debonding for these specimens (see Fig. 4c) indicate that τ_i is only marginally higher than τ_f.

It can be seen that τ_i for the TF specimens is indeed higher than the CF specimens. Within the TF specimens, τ_i for the TF-WQ specimen was higher than that for the TF-AC and TF-50C specimens. This is consistent with the observation [6] that the adhesion between the matrix and the treated fibre was better in the TF-WQ specimen where more interfacial failure into the matrix occurred.

4.6.1. Effect of fibre surface treatment conditions

The effect of fibre surface treatment conditions will now be considered. The values of specimens TF-WQ, TF(4B)-WQ, and TF(4O)-WQ are as shown in Table V. According to the manufacturer's literature, heat treatment of the glass fibre at 100 °C after the silane treatment promotes silanol condensation of the coupling agent on the glass surface. This increases the bond strength between the silane and the glass (in the case of specimen TF(4O)-WQ). The manufacturer's

TABLE V τ_i and τ_f for specimens with different treatment conditions

Specimen	TF-WQ	TF(4B)-WQ	TF(4O)-WQ
τ_i(MPa)	7.5	7.3	7.1
τ_f(MPa)	2.9	2.4	2.5

literature does not contain any information on the effect of increasing the silane treatment time (4 min treatment time for specimen TF(4B)-WQ).

It can be seen from Table V that both the heat treatment of the fibre and long silane treatment times have little effect on τ_i and τ_f. This indicates that the above two factors have little effect on the properties of the composite. It is not surprising that improved adhesion between the PP and the glass fibre arising from the heat treatment does not affect the interfacial properties because failure occurs [6] predominantly around the matrix–silane interface and not around the silane–fibre interface. Moreover, a longer silane treatment time does not affect the nature or thickness of the silane layer [5].

4.7. Comparison of experimental and theoretical curves

Theoretical plots of F_d versus L were generated by substituting the appropriate interfacial parameters in Tables III and IV for each specimen into Equation 1. These theoretical plots are as shown in Fig. 9a–f. It can be seen from Fig. 9 that there is good agreement between the theoretical and experimental data. This indicates that the model utilized for determining the interfacial parameters is reliable.

5. Conclusions

The proposed model [1] for the single-fibre pull-out test provides a simple means to evaluate four interfacial parameters from one set of pull-out data. These interfacial parameters include the interfacial shear strength, τ_i, the interfacial frictional stress, τ_f, the interfacial coefficient of friction, μ, and the matrix shrinkage pressure on the fibre, P_0. It has been demonstrated that values of the interfacial parameters evaluated from the experimental data utilizing the model are reliable.

The interfacial shear strength, τ_i, in the untreated clean fibre specimens was very low and was similar to the respective interfacial frictional stress, τ_f. Silane treatment of the glass fibres increased the interfacial strength appreciably although the final value of τ_i was still low. Both the interfacial coefficient of friction, μ, and the interfacial frictional stress, τ_f, were higher for the silane treated specimens than for the untreated fibre specimens. The above observations indicate that the silane-treated glass fibre–PP specimens have higher strength and toughness because of the higher values of τ_i, τ_f and μ.

The matrix shrinkage pressure, P_0, was only dependent on the cooling rate of the specimen during processing. For the glass fibre–PP system considered, the mechanical properties of the composite were not affected by the improved adhesion between the fibre and the matrix obtained by heat treatment of the silane-treated fibre.

Acknowledgement

One of us (W.L.C.) is grateful to the University of Hong Kong for financial support during the course of this work.

References

1. C. Y. YUE and W. L. CHEUNG, *J. Mater. Sci.* **27** (1992) 3173.
2. B. CUNNINGHAM, J. P. SARGENT and H. K. G. ASHBEE, *ibid.* **16** (1981) 620.
3. P. S. CHUA and M. R. PIGGOTT, *Compos. Sci. Tech.* **22** (1985) 185.
4. P. B. BOWDEN, *J. Mater. Sci.* **5** (1970) 517.
5. W. L. CHEUNG, PhD thesis, University of Hong Kong (1990).
6. C. Y. YUE and W. L. CHEUNG, *J. Mater. Sci.* **26** (1991) 870.
7. R. T. DeHOFF and F. N. RHINES, in "Quantitative Microscopy" (McGraw Hill, New York, 1968) Ch. 7.
8. W. L. CHEUNG and C. Y. YUE, *Polym. Commun.* **31** (1990) 96.
9. C. Y. YUE and W. L. CHEUNG, *J. Mater. Sci. Lett.* **10** (1991) 1335.

Received 6 June
and accepted 31 October 1991